RSC Advances

PAPER

View Article Online
View Journal | View Issue

Cite this: *RSC Adv.*, 2026, **16**, 14778

Converting waste into a resource: ethylenediamine modification of iron blast furnace slag to fabricate a cost-effective adsorbent for effective Pb(II) removal

Wesam Abd El-Fattah,[a] Ahlem Guesmi, *[a] Rana Yahya,[b] Ahmed M. Alharbi,[c] Naoufel Ben Hamadi,[a] Ahmed M. Eldesoky[de] and Reda F. M. Elshaarawy *[f]

The current study represents a new and cost-effective approach to fabricate a potential scavenger for adsorptive removal of Pb(II) from wastewater. Blast furnace slag, a byproduct of the iron manufacturing process, was employed as a key starting material for fabricating an ethylenediamine-functionalized adsorbent (NN@Slag). The spectral, microscopic and N_2-absorption analyses revealed the porous network of NN@Slag and the distribution of amine groups on the NN@Slag surface. The newly developed adsorbent demonstrates a strong potential for removing Pb(II) ions from wastewater, achieving a peak adsorption capacity of 108.04 mg g^{-1} under optimal conditions: a pH of 6, a contact time of 90 min, a dosage of 0.04 g NN@Slag, and an initial Pb(II) concentration of 100 mg L^{-1}. The EDX spectra and mapping confirmed the effective adsorption of Pb(II) onto NN@Salg. The fitting of Pb(II) adsorption data onto the NN@Slag adsorbent exhibited a strong alignment with the Langmuir model (R^2 = 0.98998) and pseudo-second order (PSO) kinetic model (R^2 = 0.98544), indicating that the adsorption process is predominantly governed by a monolayer adsorption mechanism and is significantly influenced by chemisorption.

Received 26th January 2026
Accepted 6th March 2026

DOI: 10.1039/d6ra00707d

rsc.li/rsc-advances

1 Introduction

The discharge of industrial waste containing heavy metal ions (HMIs) results in water pollution, presenting a significant global environmental challenge. A frequent HMI found in many industrial aqueous effluents is lead, which is generally dangerous (*e.g.*, battery manufacture, metal plating, paint, acid rock drainage, ceramic and glass sectors).[1,2] Lead exposure can disrupt biological processes, including hemoglobin synthesis, blood pressure regulation, and renal function, potentially causing kidney failure. It is associated with adverse reproductive outcomes like miscarriages and stillbirths. Of particular concern is its impact on neurological development, causing brain damage and impairing cognitive abilities in children.[3,4] Consequently, the scavenging of Pb from wastewater is of considerable importance and has extensive effects. The imperative to mitigate Pb contamination in water sources has driven the development of various treatment technologies, including solvent extraction, chemical precipitation, membrane filtering, ion-exchange resins, co-precipitation, and adsorption.[5,6] Nevertheless, the initial four techniques exhibit certain deficiencies: they frequently achieve only partial purification, necessitate substantial quantities of chemicals or energy, and result in the production of hazardous sludge that requires additional management.[5] As a result, with growing focus on economic and environmental issues in recent years, sorption has emerged as a more feasible and cost-effective process compared to other remediation techniques.

Various low-cost and safe adsorbents have been developed for lead ions removal, such as natural goethite,[7] monoliths clay,[8] bentonite clay,[9,10] chitin,[11] phosphorylated chitin,[12] iron-coated sand,[13] algae,[14] lignite,[15] zeolite,[16] brown seaweed,[17] sawdust,[18] olive stone waste,[19] coal fly ash,[20] furnace steel dust,[21] fly ash bagasse,[22] red Mud,[23] blast furnace slag,[24] agro-waste,[25] and chitosan.[26] Nonetheless, their wide applications are constrained due to factors such as relatively low efficiency and challenges in using a very fine powdered form that often remains suspended and is hard to retrieve.[27] Consequently, the

[a]*Chemistry Department, College of Science, Imam Mohammad Ibn Saud Islamic University (IMSIU), P. O. Box 5701, Riyadh, 11432, Saudi Arabia. E-mail: amalkasme@imamu.edu.sa*

[b]*University of Jeddah, College of Science, Department of Chemistry, Jeddah, Saudi Arabia*

[c]*Department of Chemistry, Faculty of Sciences, Umm Al-Qura University, Makkah, Saudi Arabia*

[d]*Department of Chemistry, University College in Al-Qunfudhah, Umm Al-Qura University, Al-Qunfudhah 21912, Saudi Arabia*

[e]*Chemical Engineering Department, High Institute of Engineering &Technology, New Damietta 34517, Egypt*

[f]*Department of Chemistry, Faculty of Science, Suez University, 43533 Suez, Egypt. E-mail: reda.elshaarawy@suezuniv.edu.eg*

development of efficient, affordable, recyclable, and environmentally friendly adsorbents for treating the lead-contaminated wastewater has become critically important.

Currently, the expansion of the steel and construction materials sectors has led to the steel manufacturing industry generating large amounts of solid by-products. Among these, blast furnace slag (BFS) is the primary by-product formed during the iron-making process in blast furnaces. BFS represents 30% of the total pig iron production, translating to a minimum of 418.8 million tons.[28] The US Geological Survey Mineral Commodity Summaries project that the global output of blast furnace slag will reach 445.6 million tons by the year 2030.[28] BFS primarily consists of metal oxides including Fe_2O_3, CaO, and SiO_2, along with other oxides such as Al_2O_3 and MgO, as well as trace amounts of metallic elements including V, Ti, and Mn.[29] Despite a significant amount of BFS has been used as a supplementary cementitious material, a considerable amount still unused and disposed into landfills, a considerable amount still unused and disposed into landfills where it not only contributes to environmental degradation but also represents a missed opportunity for resource recovery.[28] Therefore, it is crucial to develop sustainable recycling approaches and utilization strategies for BFS.

Over recent years, much effort has focused on developing amine functionalized adsorbents to treat heavy metal polluted waters. Silica,[30] carbon materials,[31,32] clays,[33] fly ash,[34] and industrial waste[35–37] have been treated with mono and polyamines (*e.g.* aminopropyl, ethylenediamine diethylenetriamine, or triethylenetetramine) using silane coupling again polymer coating or co-precipitation, producing sorbents capable of forming stable inner sphere complexes with Pb(II) and other cations. Studies have shown that metal affinity improves, and selectivity can be achieved upon incorporating nitrogen donor groups in ligands, while uncovering similar limitations: multi-step activation or acid leaching protocols; dependency on expensive precursors; fine powdered products difficult to separate from treated water; modest recyclability under realistic regeneration conditions. While most previous work into waste-derived adsorbents has focused on coal fly ash, desulfurization ash and coal gasification slag, BFS remains an underexplored platform for organic functionalization despite its vast global production and Ca/Fe-rich highly basic mineralogy.

In this regard, the current investigation proposes NN@Slag as a process-oriented improvement, which focuses on that particular gap. Unlike previous studies where multi-step coatings were required, prior acid leaching was performed or high temperature activation was employed, we used only BFS as an inorganic precursor and single step post-grafting of *N*(3 (trimethoxysilyl)propyl)ethylenediamine under mild conditions. The resulting granular, mechanically stable adsorbent retains the native mesoporous slag architecture while surface $-NH_2$/–NH donor sites become accessible on its surface. We emphasize that our approach (i) focuses on a converter blast furnace slag (BFS), which has an extensive documentation and rapidly growing global stock, (ii) employs a one-pot, post grafting approach using *N*(3-(trimethoxysilyl)propyl)ethylenediamine compatible with large scale, solvent based treatment of surfaces already practiced at large scale in industry and; (iii) results in production of a granular adsorbent that is mechanically stable to handling and that can be filtered and regenerated without the handling issues typical for fine mineral or carbonaceous powders. These features: (i) the nature of the waste stream; (ii) the simplicity and scalability of the functionalization, enabling its use as a highly dispersed material; and ultimately (iii) practical "form factor" of this adsorbent, constitute the essence of innovation in this study. By combining an overlooked high-volume waste (BFS), a technically straightforward ethylenediamine functionalization, and demonstrable reusability, NN@Slag bridges the gap between high-performance but costly engineered sorbents and raw slags or ashes that lack sufficient capacity and stability, thereby offering a realistic and scalable route for heavy-metal remediation in large-throughput applications

2 Materials and methods

2.1. Chemicals and instrumentations

The reagents and solvents used in this were provided by the chemical suppliers and used without purification. The specifications of these chemicals were presented in the SI. Additionally, all instrumentations used for the characterization of new materials are fully described in the SI. A stock Pb(II) solution (1000 mg L^{-1}) was prepared by solubilizing the Pb(II) precursor in ($Pb(NO_3)_2$) in deionized water (DIW). To obtain serial concentrations of Pb(II) solutions, stock solution was further diluted by DIW (18.2 MΩ cm^{-1}). During adsorption experiments, the pH level was adjusted using either 0.1 M HCl or 0.1 M NaOH standard solution.

2.2. Blast furnace (steel) slag

The slag utilized in this study is BFS, sourced from a steel production facility in the industrial zone, Suez-Hurghada Road, Ain Sokhna, Suez, Egypt. The chemical composition of slag was investigated by X-ray fluorescence (XRF) analysis, as depicted in Table 1. After sieving the slag, the size fraction 75–850 μm that obtained from this process was heated to 100 ± 5 °C for 24 h, and thereafter allowed to cool to room temperature.

2.3. Synthesis of amino-functionalized slag (NN@Salg)

The BFS was thoroughly rinsed with DIW under string for an hour, then gathered through filtration and repeatedly washed with DIW and ethanol until the supernatant achieved a pH of 7. Following drying at 100 °C for 24 h, the slag was sieved to eliminate coarse particles, affording pristine slag. This slag was further modified by the post-grafting approach using *N*-(3-(trimethoxysilyl)propyl)-ethylenediamine (TMSPen) as the grafting agent. In brief, 2 g of slag was dispersed in 50 mLof anhydrous toluene under ultrasonic irradiation for 15 min. Concurrently, a solution of the grafting agent was prepared by dissolving 3 mL of TMSPen in 25 mL of anhydrous toluene. Subsequently, the grafting agent solution was incrementally introduced into the slag solution under vigorous stirring, and the resultant mixture was subjected to reflux with continuous

stirring for a duration of 12 h. Finally, the modified slag was filtered, washed with anhydrous toluene to remove the residual unreacted TMSPen and then dried at 110 °C for 24 h.

2.4. Adsorption studies

2.4.1. Investigations using batch adsorption. Batch experiments play a pivotal role in investigating the efficacy of any new absorbent in removing its targeted pollutant. These experiments were conducted under different conditions by varying the pH level, adsorbent dose, adsorption time, initial pollutant concentration, and solution temperature, to adapt the optimum conditions required for the new absorbent to achieve maximum removal efficacy. In this context, a series of batch experiments were performed by exposing of NN@Salg adsorbent lead(II) ion solutions under different serial conditions to evaluate its adsorption performance. Initially, analytical grade $Pb(NO_3)_2$ was used as a precursor to prepare a stock solution of Pb(II) ions (1000 ppm), which was then gradually diluted to prepare Pb(II) solutions of serial concentrations. Pb(II) concentration was estimated prior to and following the adsorption process using the atomic adsorption spectrometry (AAS). The equilibrium adsorption capacity (q_e) and efficiency of Pb(II) removal (E%) were computed utilizing formulas (eqn (1), and (2)), respectively:

$$q_e = \frac{([Pb]_i - [Pb]_e) \times \text{volume of sample(L)}}{\text{mass of biosorbent(g)}} \quad (1)$$

$$E\% = \frac{[Pb]_i - [Pb]_e}{[Pb]_i} \times 100 \quad (2)$$

2.4.1.1 pH. The pH range of 1.0–8.0 was used to evaluate the impact of pH on the Pb(II) ion uptake by the new adsorbent. A set of batch adsorption experiments were conducted by adjusting the pH level within this range using adsorbent dose of 0.03 g and 50 mL of Pb(II) solution with initial concentration of 100 ppm. The adsorption contact time was maintained at 60 min and a temperature of 298 K. Standard HCl (0.1 M) or NaOH (0.1 M) solutions were used to adjust the pH level of sample. At the end of experiment, the adsorbent was removed filtration through a 0.45 μm syringe filter. After that, the free Pb(II) ion in filtrate was analyzed using AAS.

2.4.1.2 Contact time. Batch experiments were conducted at the predetermined optimal pH value and under the experimental conditions outlined in the previous section to investigate the effect of adsorption contact time, ranging from 5 to 200 minutes, on the uptake of Pb(II) ions by NN@Salg. At the end of the adsorption experiment, the adsorbent was collected by filtration through a syringe filter (0.45 μm). After that, AAS was used to periodically analyze the free Pb(II) ions in the filtrate. Eqn (3) was employed to estimate the Pb(II) uptake by the NN@Salg adsorbent, q_t (mg g^{-1}), at time interval.

$$q_t = \frac{([Pb]_i - [Pb]_t) \times \text{volume of sample(L)}}{\text{mass of biosorbent(g)}} \quad (3)$$

2.4.1.3 Adsorbent dose. This study examined the impact of adsorbent dose (0.01–0.05 g) on the Pb(II) removal efficiency of NN@Salg. This investigation was conducted under optimal pH and time conditions. The experiments utilized a Pb(II) solution with an initial concentration of 100 ppm at 298 K.

2.4.1.4 Initial concentration. To determine the optimal Pb(II) concentration, aqueous Pb(II) solutions of serial concentrations (10–300 ppm) were subjected to batch adsorption experiments containing ions at the predetermined optimal pH, contact time, and adsorbent dose levels, while keeping temperature at 298 K.

2.4.1.5 Effect of temperature. To assess how temperature influences the adsorption capacity of NN@Salg, a series of experiments were conducted. These experiments were performed at temperatures ranging from 25 to 55 °C, adhering to the predetermined optimal conditions throughout.

2.4.2. Adsorption kinetic. By analyzing the kinetics of Pb(II) adsorption by the NN@Salg adsorbent through the evaluation of batch adsorption experiments using various kinetic models, we can gain valuable insights into the effectiveness and mechanism of this adsorption process.[38,39] In this context, the batch adsorption experiment was conducted using 50 mL of Pb(II) solution (80 ppm) under optimum conditions: pH = 6, adsorbent dose = 0.03 g, temperature = 50 °C. Thereafter, samples of the adsorbate solution were taken at specified time intervals (from 0 to 120 min), filtered through a 0.45 μm syringe filter, and then analyzed to measure the residual free Pb(II). The adsorption experiment findings were examined using pseudo-first order (PFO), pseudo-second order (PSO), and intraparticle diffusion (IPD) kinetic models (refer to Table S1, SI)[32] to elucidate the sorption mechanism.

2.4.3. Sorption isotherms. Initially, Pb(II) solutions of serial concentrations ranging from 0 to 500 mg L^{-1} were used to construct calibration curve. After that, batch adsorption experiments were performed under optimal conditions using Pb(II) solutions of serial concentrations. After performing batch experiments and removing adsorbent by filtration, the filtrate was analyzed to quantify the free Pb(II) ion. The study of Pb(II) adsorption onto the NN@Salg adsorbent was conducted using three well-established isotherm models: Freundlich, Langmuir, and Temkin (refer to Table S1, SI).[40]

2.4.4. Recovery and recyclability. The new adsorbent's recovery and reusability were examined by performing several adsorption–desorption runes using 0.1 M HNO_3 solution as a desorbing agent. Following each adsorption run, the adsorbent was collected by filtration through a 0.45 μm syringe filter and subsequently washed with deionized water (DIW). The

Table 1 The chemical composition of the received steel slag

Elements	CaO	SiO_2	Fe_2O_3	MgO	Al_2O_3	MnO	P_2O_5	Na_2O	Cr_2O_3	V_2O_5	TiO_2
Content (wt%)	32.90	15.26	34.41	6.62	6.65	2.05	0.39	0.11	0.42	0.24	0.67

regeneration of the adsorbent was performed by agitating isolated precipitate with 0.1 M HNO_3 solution (1 : 10 w/v) at 60 °C for 30 min. The regenerated adsorbent was collected by centrifugation followed by filtration and then meticulously rinsed with DIW prior to being used for the subsequent adsorption cycle. On the other hand, AAS was utilized to measure the liberated Pb(II) and desorption efficiency (DE) using eqn (4):

$$\mathrm{DE}(\%) = \frac{[\mathrm{Pb}]_i}{[\mathrm{Pb}]_i - [\mathrm{Pb}]_{free}} \times 100 \quad (4)$$

3 Results and discussion

3.1. Characterization of pristine and amino-functionalized steel slag (NN@Slag)

The XRF (X-ray fluorescence) analysis (Table 1) confirms that the BFS is primarily composed of CaO (32.90 wt%), Fe_2O_3 (34.41 wt%), SiO_2 (15.26 wt%), MgO (6.62 wt%), and Al_2O_3 (6.65 wt%). This composition is characteristic of BFS, which typically exhibits high alkalinity and metal oxide content, making it intrinsically reactive toward acidic pollutants and heavy metal cations.[41] The abundance of Ca^{2+} and Fe^{3+} ions suggests potential for ion exchange and surface complexation, although unmodified slag often suffers from low selectivity and slow kinetics for specific metal ions like Pb(II).[42]

XRD patterns (Fig. 1) of both pristine and modified slag reveal crystalline phases typical of BFS, including larnite (β-Ca_2SiO_4, JCPDS 33-0302), brown millerite ($Ca_2(Al,Fe)_2O_5$), and wüstite (FeO). The lack of new crystalline peaks in NN@Slag indicates that the functionalization process is surface-limited and does not induce phase transformation, a critical feature for maintaining mechanical stability while introducing new surface chemistry.[43]

Notably, the XRD patterns for pristine converter slag and NN@Slag show not only sharp reflections due to crystalline phases (*i.e.*, larnite, brownmillerite, and wüstite), but also a diffuse background consistent with an important amorphous component. This crystalline–amorphous two-phase nature is indicative of a disordered Ca–Si–Fe supersaturated glassy phase.[44] The presence of this amorphous fraction directly affects the textural and sorption properties of NN@Slag. A such partially depolymerized, vitrified silicate network generally provides a high density of surface hydroxyl groups (≡Si–OH, ≡Fe–OH, ≡Ca–OH) and defect locations providing anchoring points for the grafting of silanes[45] and potential coordination sites for Pb(II). This is in line with the observed mesoporous nitrogen sorption behavior, moderate BET surface area and presence of ethylenediamine layer as inferred from FTIR, XPS and EDS analyses. By explicitly acknowledging the significant amorphous contribution, we are now able to present a much more realistic structural image in which both crystalline phases and disordered matrix cooperatively govern surface chemistry, roughness and accessible area-elements that collectively underlie the high Pb(II) uptake and robust performance of NN@Slag.

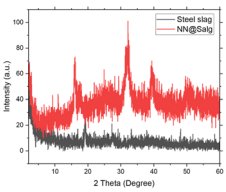

Fig. 1 The XRD of the steel slag before and after modification.

Fig. 2 illustrates the SEM analysis of the morphological and microstructural characteristics of the modified slag (NN@Slag). The NN@Slag clearly exhibited an irregular architecture with a porous configuration, which increased the specific surface area and offered more active sites for Pb(II) adsorption. This, in turn, allowed Pb(II) ions to diffuse onto the steel slag surface and improved the NN@Slag's adsorption capability.

As shown in Fig. 3, the EDS analyses of NN@Slag show a thorough elemental composition that not only validates the presence of major slag elements like Fe, Mn, and O, but also shows that the silyl-propyl ethylenediamine group was successfully grafted, as evidenced by the detection of C, O, and Si peaks. It is important to note that the nitrogen (N) peak is not present in the EDS spectrum, which could be due to several factors.[46,47] EDS is less sensitive to light elements like nitrogen because X-ray emissions are weak in normal SEM conditions. The concentration of nitrogen on the surface from ethylenediamine may not be very high, which could make the signal less strong. Also, nitrogen detection could be hard because of signal overlap from nearby peaks and matrix effects. Despite this, the presence of C and Si peaks serves as a strong indicator of the successful modification of the slag surface with the silyl-propyl ethylenediamine group.

Fig. 3 displays the EDS results for NN@Slag after Pb(II) adsorption, which reveals a significant change in the elemental composition of NN@Slag post-adsorption process. The elemental mapping show lead spread evenly across the NN@Slag surface, suggesting the NN@Slag adsorbs Pb(II) quite efficiently under optimal conditions. The EDS spectrum also shows clear Pb peaks that were nowhere to be found in the original, native NN@Slag. At the same time the usual slag constituents, Fe, Mn, Si, O and C, still observed. This combination of new Pb signals together with steady Si and Fe lines may indicate that the slag framework stayed stable after the adsorption process. Similar findings have been documented in related studies of amine-functionalized adsorbents, where Pb(II) adsorption is corroborated through elemental mapping and spectral analysis,[2,6] revealing enhanced Pb signals superimposed on the base adsorbent elements, thereby validating surface complexation and adsorption efficiency. These results collectively demonstrate that NN@Slag effectively captures Pb(II) through surface functional groups without compromising adsorbent integrity, underscoring its potential for practical heavy metal remediation. The adsorption mechanism is primarily attributed to chelation/complexation between Pb(II) ions and the amine/imine groups (–NH_2/–NH–) of the grafted ethylenediamine ligand. Pb(II), a soft Lewis acid, exhibits high affinity for soft Lewis bases like nitrogen donors, forming stable

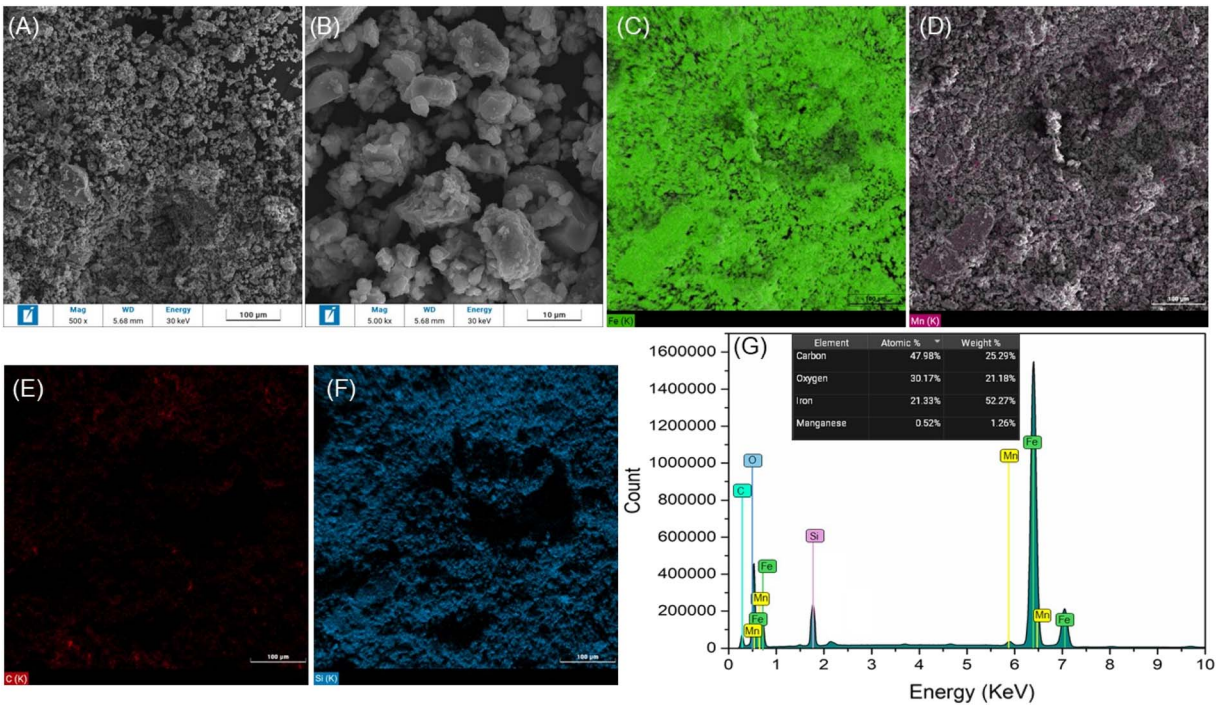

Fig. 2 (A and B) SEM images, (C–F) color-coded elemental maps, and (G) EDS spectrum of the new adsorbent (NN@Slag) before uptake of Pb(II). The inset in panel 3G shows quantitative atomic and weight percentages.

five- or six-membered chelate rings.[48] This is consistent with previous studies on amine-functionalized silica, polymers, and biochars for Pb(II) removal.[49]

Fig. 4 displays the N_2 adsorption–desorption isotherms for both the pristine slag and its modified counterpart (NN@Slag). According to the classification by the IUPAC standards, the nitrogen adsorption isotherm of the slag samples aligns with the standard type II isotherm. This alignment suggests that the slag samples exhibit a mesoporous structure.[50] Furthermore, it was observed that the isotherms of the slags demonstrated

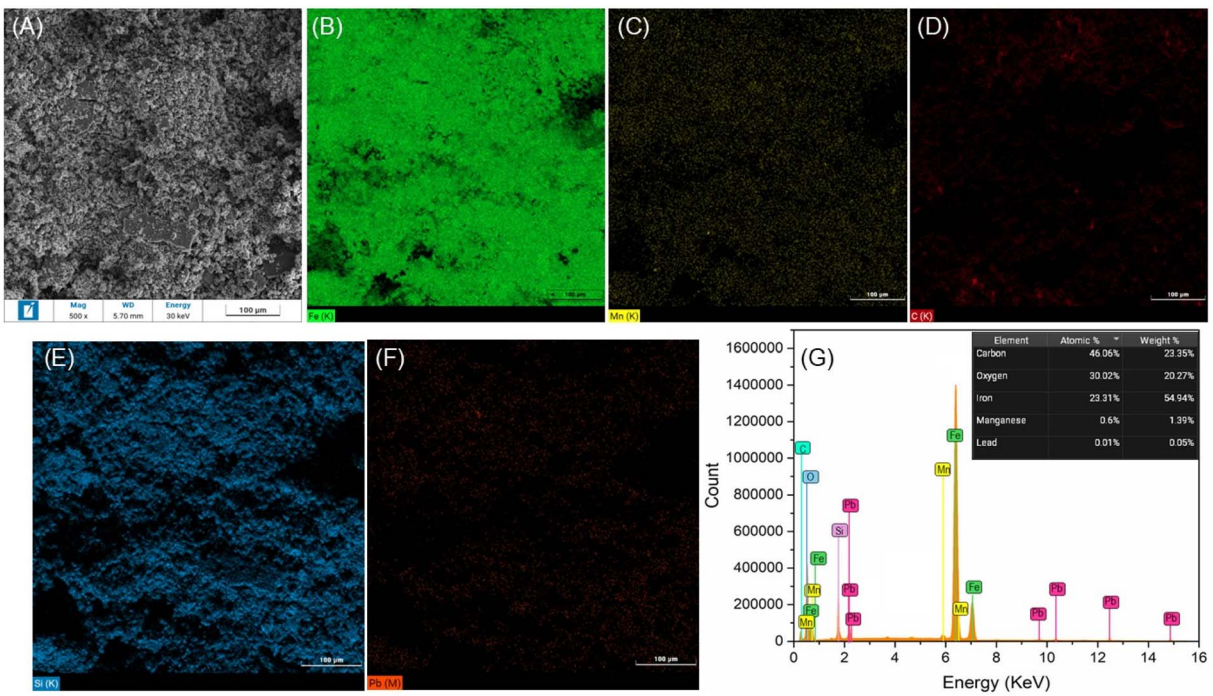

Fig. 3 (A and B) SEM images, (C–F) color-coded elemental maps, and (G) EDS spectrum of the new adsorbent (NN@Slag) before uptake of Pb(II). The inset in panel 4G shows quantitative atomic and weight percentages.

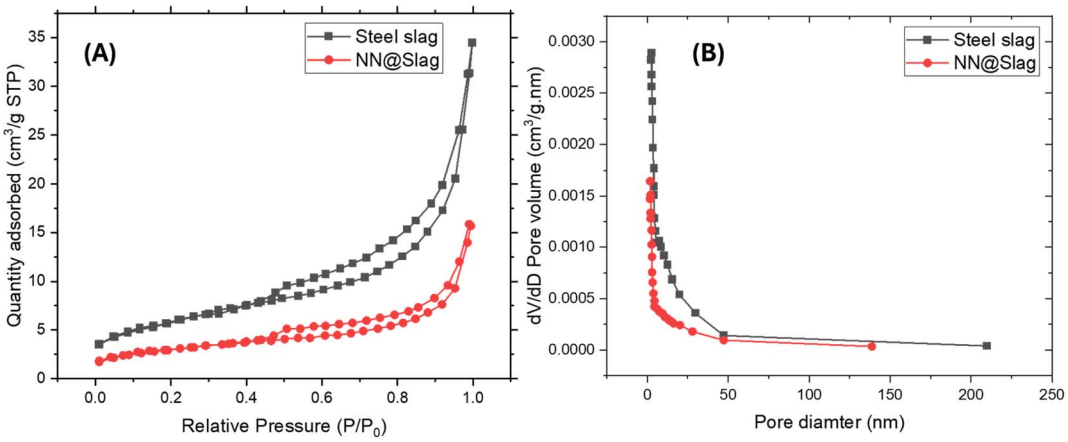

Fig. 4 (A) N_2 adsorption–desorption isotherm and (B) pore size distribution of the steel slag and the modified steel slag (NN@Slag).

a characteristic HIII-type hysteresis loop, suggesting that the slag constituted a layered aggregate.[51] Also, the NN@Slag exhibited a relatively low specific surface area of 11.82 $m^2\ g^{-1}$ as compared to the pristine slag sample (21.79 $m^2\ g^{-1}$). This may be attributed to the silane coupling agent coating the surface of the slag. Furthermore, as illustrated in Fig. 5B, the pore size distribution analysis indicated that both slag and modified slag (NN@Slag) demonstrated a singular peak within the microporous region, approximately at 1.69 nm.

3.2. Adsorption studies

To optimize the protocol for the efficient scavenging of Pb(II) ions using a novel adsorbent, the parameters controlled in the Pb(II) uptake using NN@Slag should be fine-tuned and optimized. Therefore, it is crucial to study the impacts of various

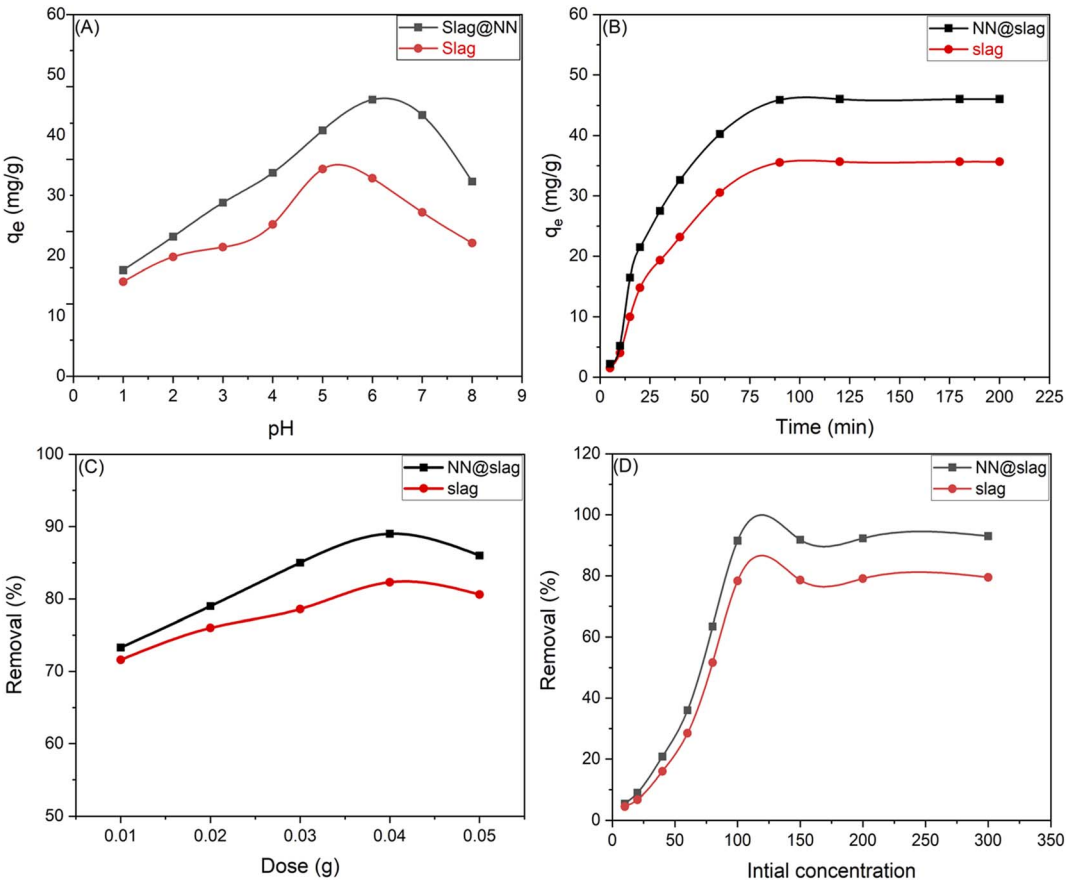

Fig. 5 Effects of various parameters such as pH (A), adsorption time (B), sorbent dose (C), and initial concentration of Pb(II) (D), on the Pb(II) uptake by NN@Slag in comparison to the pristine slag at 25 °C.

parameters (pH, time, adsorbent dose, initial Pb(II) concentration, and temperature) on the adsorption capacity NN@Slag. This to determine the optimal level of each parameter, to achieve maximum removal efficiency.

3.2.1. Effect of pH. The pH level of the adsorbate (Pb(II)) solution determine the form of Pb(II) exist in the solution and influences the resulting sorption or precipitation processes. Consequently, it is important to maintain the pH at optimal level to achieve a maximal removal efficiency. Fig. 5A illustrates that the Pb(II) uptake by both slag and NN@Slag was relatively minimal when the pH value ranged from 1 to 3. Nonetheless, the adsorption capacity of NN@Slag was remarkably enhanced with pH elevation to reach maximal level (q_e = 45.9 mg g^{-1}) near-neutral pH (6). In contrast, pristine slag reached its peak q_e of 34.37 mg g^{-1} at pH 5, with lower adsorption at higher pH likely due to surface charge and precipitation effects. Two reasonable factors are responsible for the significantly low adsorption capacity of NN@Slag in a strongly acidic medium (pH = 1–3). First, there is strong competition for the accessible active binding sites on the NN@Slag surface between the large population of protons and Pb(II) cations. Additionally, protonation of the amine groups on the NN@Slag surface, resulting in a positively charged surface that repels Pb(II) cations and reduces adsorption efficiency.[52] These groups deprotonate as the pH rises, creating a negatively charged adsorbent surface that promotes complexation with Pb(II) cations and electrostatic attraction, increasing the adsorption capacity. This interaction is typically optimized at pH values close to neutral, which maximizes Pb(II) uptake. Importantly, as the solution approaches neutrality, Pb(II) speciation will shift toward partial precipitation of $Pb(OH)_2$. The reduction in dissolved Pb(II) is attributed to the specific adsorption on NN@Slag and hydroxide precipitation rather than mere adsorption. It is consistent with the previous reports that biosorption/adsorption of Pb(II) can occur simultaneously with precipitation of $Pb(OH)_2$ at neutral to weak alkaline pH.[12,20,53] When the pH rises above 7, hydrolyzed species such as $Pb(OH)^+$ and $Pb(OH)^2$ can form.[54] These species can precipitate out of solution, thereby decreasing the adsorption efficacy. More on the disentanglement of these contributions will be addressed in future work.

3.2.2. Effect of contact time. The kinetics of the adsorption process are crucial for understanding the efficiency of an adsorbent. In this context, the influence of varying adsorption contact times, from 5 to 200 min, on the absorption of Pb(II) was studied. As illustrated in Fig. 5B, the Pb(II) uptake by NN@Slag increased with increasing time, reaching equilibrium within 90 min (q_e = 46.09 mg g^{-1}), which is faster and higher than the pristine slag (q_e = 35.61 mg g^{-1}). This enhanced kinetic behavior results from the increased active sites and affinity introduced by ethylene diamine functionalization, which facilitates more efficient interactions with Pb(II).

3.2.3. Effect of adsorbent dose. Because the adsorbent dosage changes the surface area and available active sites, it has a significant impact on the adsorption kinetics and equilibrium capacity. Due to increased adsorption site availability and faster initial adsorption, increasing dosage improves removal efficiency. On the other hand, because of site overlapping, particle aggregation, and possible site unsaturation, overdosage can reduce adsorption capacity per unit mass. Therefore, optimizing the dose of adsorbent is important to attain maximal scavenging efficacy and adsorption capacity. Fig. 5D shows a direct correlation between the adsorbent dose and removal efficiency, with an optimal dosage of 0.04 g resulting in a maximum removal efficiency of 89.16% for NN@Slag, which exceeds the 83.14% efficiency recorded for slag. This indicates that NN@Slag is more effective at lower dosages, which is economically beneficial for large-scale applications. It worth noted that, beyond the optimal dose, further increase in the adsorbent dose results in efficiency decline.

3.2.4. Effect of initial concentration. To enhance adsorption efficiency and develop successful remediation protocol, it is crucial to study and understand the impact of the initial Pb(II) concentration on the adsorbent uptake. This understanding can help establish guidelines to limit Pb(II) levels in contaminated water sources to be treated, thereby reducing the risk of lead contamination. Consequently, the adsorption experiments were conducted by blending optimum adsorbent dose with Pb(II) solutions of gradient concentrations (10 to 300 ppm) under optimum conditions to investigate the optimal initial concentration. Fig. 5E reveals that with an increase in the initial concentration of Pb(II), its uptake is significantly improved. Notably, at an initial concentration of 100 ppm, NN@Slag achieves a maximal removal efficiency of 91.49%, while slag shows a removal efficiency of 78.32%. Nevertheless, once the concentration exceeded 100 ppm, the efficiency of removal leveled off, signifying that the adsorbent had reached its saturation point. The improved performance at higher initial concentrations can be explained by the stronger driving force for mass transfer, which makes it easier for Pb(II) ions to move toward the adsorption sites on NN@Slag.[55] Also, modifying by ethylene diamine probably creates more binding sites that can hold more Pb(II) ions, which increases the overall adsorption capacity.

Remarkably, while the BET surface area of slag was reduced following TMSPen functionalization, the Pb(II) adsorption capacity of NN@Slag improved significantly showing that adsorption is ruled more by surface complexation sites than total gas-accessible area. This is consistent with a process controlled by chemisorption, evidenced by the good fit to the Langmuir and pseudo second-order models (see Section 3.9) and spectroscopic evidence that specific Pb–N/O coordination occurs at the modified surface. In fact, as any decrease in BET surface area caused by pore blocking by organic moieties was more than offset by the introduction of new sites that had strong binding affinities for Pb(II) that stable coordination bond formation with amine and oxygen functionality,[53] we found a high density of grafted TMSPen provided excellent binding between these heavy metals and slag network. Hence, the increase in Pb(II) uptake upon modification should be attributed to the augmented chemical reactivity and availability of these functional sites in aqueous phase rather than a mere increase in physical surface area.

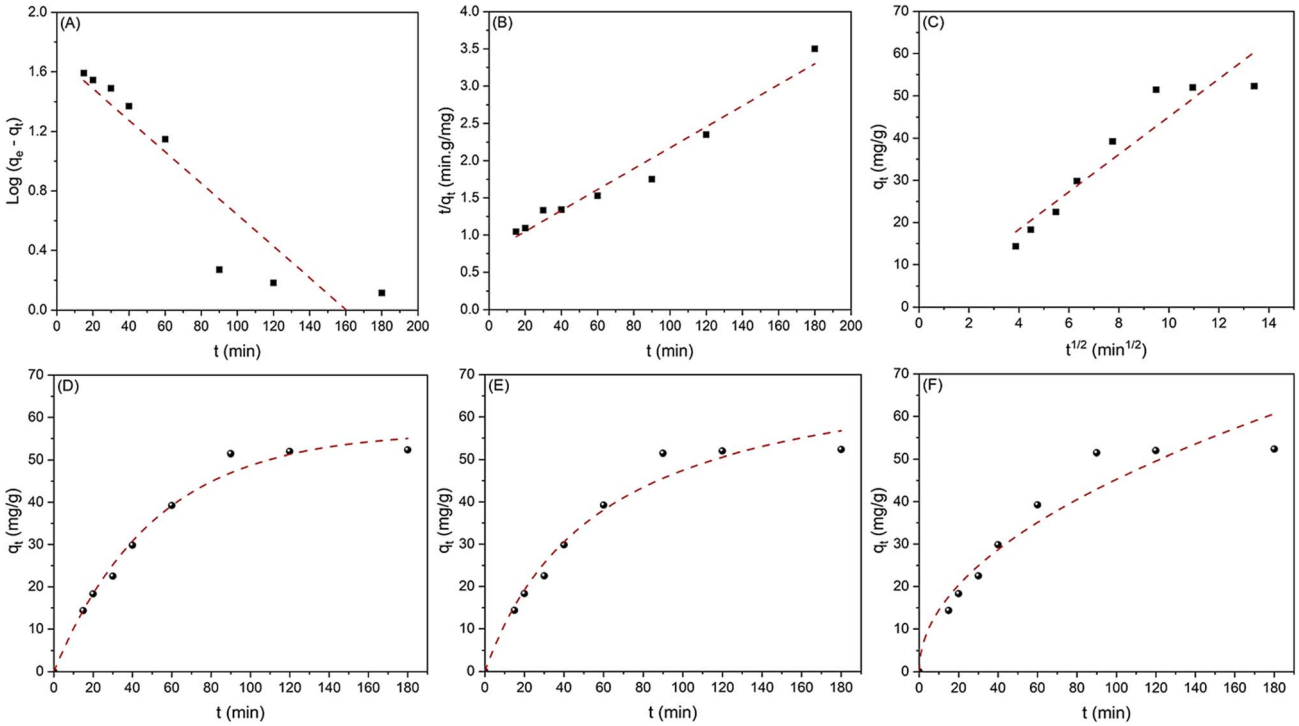

Fig. 6 (A–C) Linear and (D–F) non-linear fitting of kinetic models to the data of Pb(II) adsorption onto NN@Slag including (A and D) PFO, (B and E) PSO, and (C and F) IPD, respectively.

3.3. Adsorption kinetics

The kinetics of Pb(II) adsorption onto NN@Slag were systematically analyzed using the most common kinetic models: PFO, PSO, and IPD models, in linear and nonlinear regression style (refer to Fig. 6). According to the regression fitting parameters (Table 2), the nonlinear pseudo-second-order model emerged as the most suitable for representing the, yielding a high correlation coefficient (R^2 = 0.98544) and an equilibrium adsorption capacity (q_e) of 81.13 mg g^{-1}, outperforming the pseudo-first-order model. This value is notably higher than the adsorption capacities reported for the unmodified BFS (41.66 mg g^{-1})[56] and aminopropyl-modified BFS (40.62 mg g^{-1}).[52] Interestingly, the adsorption capacity of NN@Slag surpass that of other agro-, bio-, and industrial waste adsorbents, which typically range from 14 to 70 mg g^{-1} under comparable conditions.[27] In comparison, NN@Slag's performance is competitive, especially considering its base material as industrial slag, which is abundant and low-cost.

Table 2 Linear and non-linear fitting of the kinetic models for the data of Pb(II) adsorption onto NN@Slag[a]

	Fitting parameters						
Model		q_e (mg g^{-1})	k_1 (min^{-1})	χ^2	RMSE	COD	R^2
PFO	Linear	49.89	0.02437	0.42388	−0.92702	0.85936	0.83592
	Nonlinear	56.67	0.01958	9.82259	68.75815	0.97588	0.97254
		q_e (mg g^{-1})	k_2 x 10^{-3} (g mg^{-1} min^{-1})	χ^2	RMSE	COD	R^2
PSO	Linear	76.12	0.25766	0.16576	0.98235	0.96502	0.95919
	Nonlinear	81.13	0.22803	5.15171	36.062	0.98735	0.98544
		C (mg g^{-1})	k_{id} (mg g^{-1} $min^{-1/2}$)	χ^2	RMSE	COD	R^2
IPD	Linear	0.53344	4.4551	190.84756	0.94377	0.8907	0.87248
	Nonlinear	0.19297	4.50418	26.70358	186.92506	0.93444	0.92507

[a] χ^2 = Reduced Chi-Sqr; RMSE = residual sum of squares; COD = R-square; R^2 = Adj. R-square.

The kinetic fitting strongly favored PSO model for NN@Slag, consistent with chemisorption being the primary adsorption mechanism, a trend widely observed in heavy metal adsorption studies involving pristine and modified slags[52,57] and biochars.[58,59]

In addition to the coefficients of determination (R^2 and COD) already reported, Table 1 also provides the reduced chi-square (χ^2) and residual root mean square error (RMSE) values for all linear and non-linear fittings corresponding to the pseudo-first-order, pseudo-second-order, and intraparticle diffusion models in order to collect a more rigorous statistical validation from kinetic fits. The much smaller values of χ^2 and RMSE for the pseudo-second-order model, as well as its larger R^2/COD, further support that this model best describes the kinetics of Pb(II) adsorption onto NN@Slag and suggests a predominantly chemisorption-controlled process.

It is important to note that while the Pb(II) uptake data fit exceptionally well with a pseudo-second-order model, which describes chemical absorption kinetics, the Weber–Morris intraparticle diffusion plots are multi-linear and lines do not pass through the origin, indicating that intraparticle diffusion was involved in Pb(II) uptake on NN@Slag but was not the only rate-controlling step.[60] Therefore, overall kinetics are better described by a mixed-control mechanism in which external film diffusion, progressive diffusion into particle interiors and surface chemisorption act sequentially or concurrently as additives to the rate, consistent with the predominance of the pseudo-second-order model and inability of intraparticle diffusion alone to represent observed rate.

3.4. Adsorption isotherms

Adsorption isotherms provide important information on the equilibrium dynamics of the adsorbate–adsorbent system (Pb(II) ions-NN@Slag). Furthermore, these isotherms play a crucial role in forecasting the adsorption process, evaluating the interaction between the adsorbent and adsorbate, and determining surface coverage. Therefore, the adsorption findings were systemically modeled using both linear and non-linear formulas of Langmuir, Freundlich, and Temkin fittings models (refer to Fig. 7). Adsorption on a homogeneous surface with similar sites is assumed by the Langmuir isotherm model, and involves reversible monolayer coverage of adsorbate.[61] In contrast, a multilayer creation of heterogeneous adsorption sites, reversible forces between adsorbate molecules, and an exponential growth of adsorption capacity with sorbate concentration are the assumptions of the Freundlich isotherm model.[62] The Temkin model assumes a significant correlation between the adsorbate–adsorbent interaction and surface coverage, resulting in a linear correlation between surface coverage and adsorption energy.[63]

According to the fitting parameters depicted in Table 3, the nonlinear Langmuir model best one to describe the adsorption behavior Pb(II) adsorption on NN@Slag as evidenced by the highest correlation coefficients ($R^2 = 0.98998$) and a remarkable maximum adsorption capacity (q_{max}) of 108.04 mg g^{-1}. These findings suggest that the adsorption process is predominantly monolayer, taking place on a surface with a limited number of uniform sites. These results clearly position NN@Slag as a highly effective adsorbent in Pb(II) remediation applications,

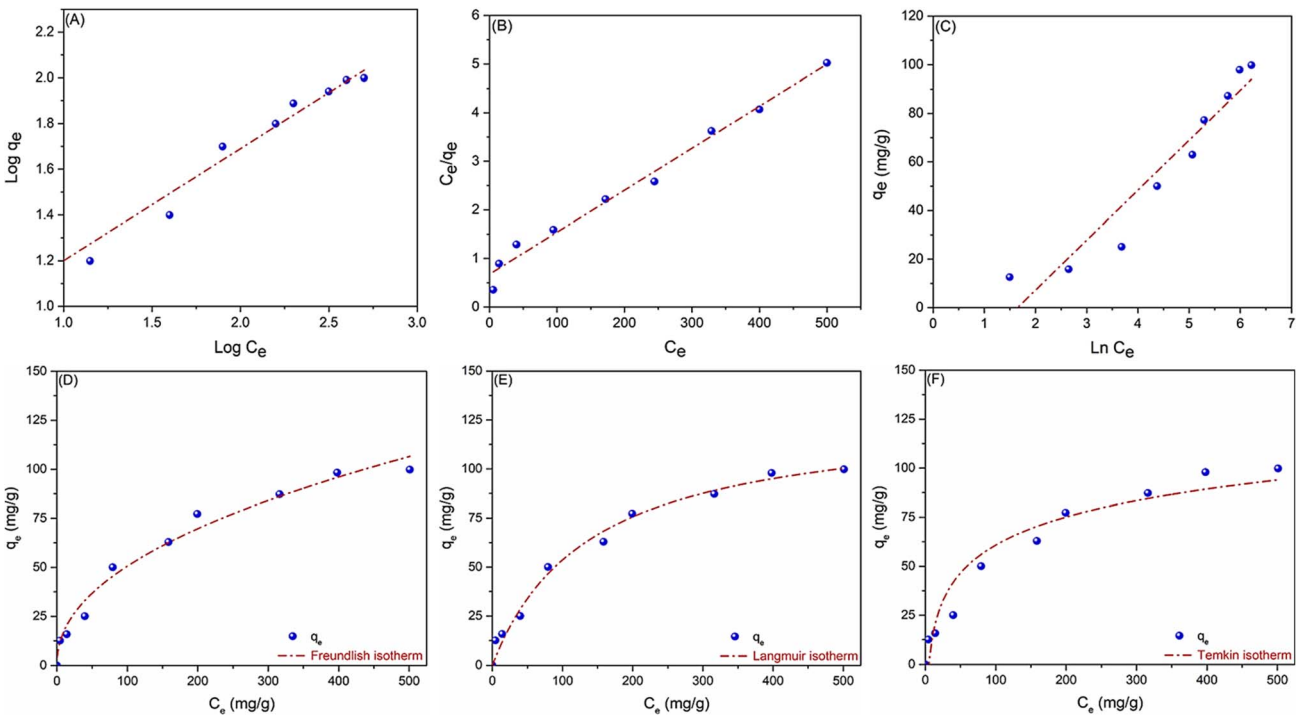

Fig. 7 (A–C) Linear and (D–F) non-linear regressions of different kinetic models including (A and D) Freundlich, (B and E) Langmuir, and (C and F) Temkin isotherm models for Pb(II) adsorption on NN@Slag.

Table 3 Linear and nonlinear fitting of the adsorption isotherms for the Pb(II) uptake onto NN@Slag

	Langmuir			Freundlich			Temkin		
Model	q_{max} (mg g^{-1})	b (L mg^{-1})	R^2	K_f (mg g^{-1})	n (L mg^{-1})	R^2	K_T (mg g^{-1})	b_T (L mg^{-1})	R^2
Linear	105.74	0.01276	0.98143	5.12224	2.03990	0.95838	0.19242	20.5697	0.90897
Nonlinear	108.04	0.00721	0.98998	6.03056	2.16464	0.96405	0.19242	20.5697	0.93233

Table 4 Thermodynamic parameters of adsorption of Pb(II) onto NN@Slag adsorbent

Temperature (°K)	$\Delta S°$ (kJ mol^{-1} K)	$\Delta H°$ (kJ mol^{-1})	$\Delta G°$ (kJ mol^{-1})	R^2
298.15	−29.44	−6.93	8.77	0.97474
303.15			8.92	
308.15			9.07	
313.15			9.21	
318.15			9.36	
323.15			9.51	
328.15			9.65	

outperforming many reported materials in both capacity and adsorption strength, while benefiting from the economic and environmental advantages of slag utilization.

The excellent fit to the Langmuir model ($R^2 \approx 0.99$) confirms that the uptake of Pb(II) occurs mainly by monolayer coverage on a finite number of energetically equivalent sites rather than unrestricted multilayer deposition. Such behavior is entirely consistent with the surface structure of NN@Slag, wherein grafting *N*-(3-(trimethoxysilyl)propyl)ethylenediamine onto a partially amorphous slag framework results in a population of well-defined amine/oxygen donor centers anchored to silanol and metal-oxide functional groups. This suggests that the Langmuir maximum capacity ($q_{max} = 108.04$ mg g^{-1}) may be interpreted as an estimation for the density of these available complexation sites under the given conditions, while significant values for the Langmuir affinity constant (b) indicate a strong, chemisorptive nature of the Pb(II)–surface interface. Thus, along with the pseudo-second-order kinetics and spectroscopic evidence of Pb–N/O coordination (refer to Section 3.8), the Langmuir fit supports a mechanistic picture in which Pb(II) forms stable inner-great complexes with a rather uniform set of amine-functionalized sites on NN@Slag, accounting for both its high capacity as well as efficient regenerability of the adsorbate. Notable, while comparatively high initial Pb(II) concentrations were used in these experiments to allow for clear determination of the Langmuir isotherm parameters and saturation behaviour, the strong affinity indicated by the fit suggests NN@Slag could also have potential of treating more dilute, realistic wastewater streams.

3.5. Adsorption thermodynamics

The additional thermodynamic analysis of Pb(II) uptake by NN@Slag was performed for further understanding of the nature of adsorption process which agrees well with kinetic and isothermic studies.[64] The Van't Hoff plot generated based on the equilibrium data across the investigated range of temperatures, 298–328 K shows a linear trend (Fig. S1, SI), implying that the standard thermodynamic parameters are well defined over the temperatures studied and no phase change nor significant change in adsorption mechanism occurs within this window. The enthalpy change is negative when calculated ($\Delta H° = -6.93$ kJ mol^{-1}) (Table 4), indicating that Pb(II) adsorption onto NN@Slag is an exothermic process which is consistent with the experimental decrease in different capacity at higher temperatures. This behavior aligns with most reported sorption systems of heavy metals on amine functionalized mineral and silica surfaces, where the binding of metal–ligands and electrostatic interactions normally liberate heat.

It is also important to note that the entropic contribution related to adsorption is negative ($\Delta S° = -29.44$ J mol^{-1} K^{-1}), indicating a gain of order near the solid-solution interface, as Pb(II) ions move from aqueous solution into specific coordination positions on the NN@Slag surface. This ordering is based on the partial desolvation of hydrated Pb(II) and formation of fewer flexible inner-sphere complexes with surface –NH_2/–NH as well as oxygen donors (XPS and FTIR data). In line with an exothermic process governed by specific binding and not entropy-driven physisorption, the Gibbs free energy change becomes less favorable with increasing temperature within this thermodynamic formalism. Collectively, these thermodynamic results lend credence to the notion that Pb(II) uptake by NN@Slag occurs *via* energetically favorable exothermic chemisorption at well-defined sites, reinforcing the mechanistic interpretation drawn from the Langmuir and PSO fits while underscoring the versatility of NN@Slag as an effective adsorbent for Pb(II) remediation under ambient conditions.

3.6. Effect of competing ions

To further assess the practical performance of NN@Slag under more realistic water-chemistry conditions, additional batch experiments were conducted at the optimized adsorption conditions in the presence of common coexisting cations (Na^+, Ca^{2+}, Mg^{2+}, Cd^{2+} and Mn^{2+}; 0.1 mM each). Results (Fig. 8A) indicated that the presence of common background electrolyte ions such as Na^+, Ca^{2+}, and Mg^{2+}had little effect on Pb(II) removal efficiency by NN@Slag which was retained at high levels after equilibration, while Mn^{2+} caused the most significant but still moderate inhibition for Pb(II) uptake. Such behavior is ascribed to the intense and specific coordination of Pb(II) with amino and hydroxyl functional groups on the NN@Slag surface, giving rise to a clear selectivity advantage

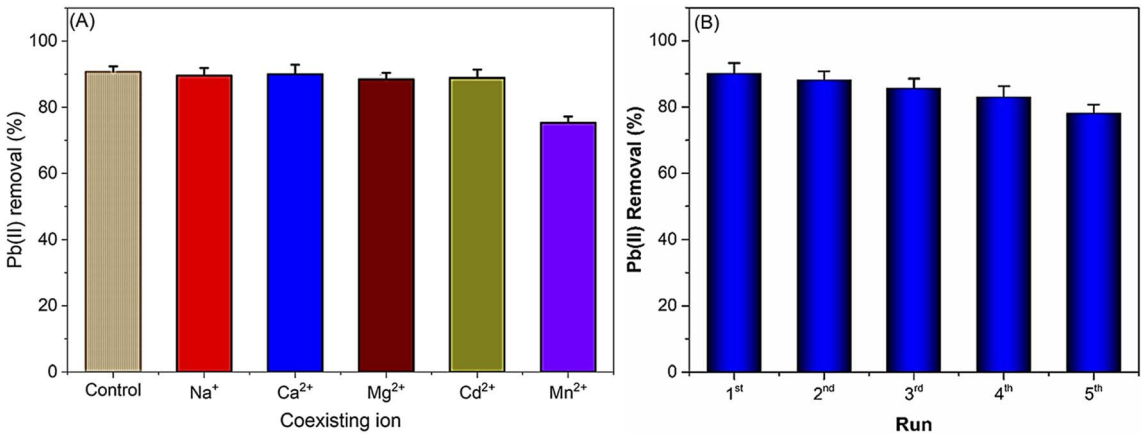

Fig. 8 (A) Effect of competing ions on the Pb(II) ions uptake by NN@Slag. (B) Reusability of NN@Slag in Pb(II) removal.

relative to lighter competing cations thus supporting the applicability of the material for Pb(II) removal from complex natural and industrial waters.

3.7. Adsorbent recovery and reusability

The recovery and reusability of adsorbents have become a focal point in environmental research. This interest is driven by the importance of improving the overall efficiency and cost-effectiveness of systems through the optimization of regeneration and recovery processes. Therefore, the potential for recovering and reusing the new adsorbent was examined by performing several adsorption–desorption cycles, utilizing HNO_3 solution as the desorbing agent. After each adsorption cycle, the adsorbent was retrieved and examined for the subsequent run. As illustrated in Fig. 8, the NN@Slag demonstrated exceptional reusability, preserving 87% of its initial adsorption efficacy after completing five sequential adsorption–desorption runs. This performance underscores its potential as a sustainable and cost-effective scavenger for water remediation. This study brings to light the significant potential of NN@Slag as an effective and sustainable adsorbent for the removal of HMIs.

3.8. NN@Slag structural integrity during adsorption–desorption cycles

FTIR (Fig. 9A) and SEM analyses (Fig. S1, SI) of fresh, Pb-loaded, and regenerated NN@Slag directly support the fact that during repeated use this new adsorbent retains its structural as well as chemical integrity. FTIR spectroscopy clearly depicts the sequential alteration of slag surface after ethylenediamine grafting, Pb(II) adsorption and subsequent regeneration. Freshly collected slag displays a broad O–H stretching band (at 3500 cm^{-1}) together with characteristic strong signals for C=O of carbonate CO_3^{2-} groups (1850 cm^{-1}), and Si–O–Si structures,[53] in the range 900–1100 cm^{-1},[65] which is typical for basic oxygen furnace slags and confirms the predominance of hydroxylated silicate and carbonate phases. Indeed, a new band appeared at 3300–3400 cm^{-1} region along with a broad band centered at 3489 cm^{-1} in combined to be attributed as the NH_2 stretching vibrations and overlapping N–H/O–H stretching peaks after functionalization of NN@Slag.[52] Additionally, the C–H stretching bands of the propyl linker were observed in the 2930–2870 cm^{-1} rang. The band located at 1594 cm^{-1} related to N–H bending of the grafted ethylenediamine, which is in good agreement with similar observations made for aminosilane modified mineral and silica surfaces.

Notable, these characteristic bands of the ethylenediamine functionality including N–H stretching, C–H stretching of the propyl linker, and N–H/C–N vibrations are clearly observed in the initial NN@Slag yet decline slightly after Pb(II) uptake (because of coordination with Pb(II)), but are essentially restored in the regenerated material after acid desorption. This reversible band intensity modulation, without band disappearance or distortion of the spectrum, suggests that the diamine layer based on ethylenediamine silane is not stripped off from the slag surface in adsorption–desorption cycles and that Pb(II) binding occurs predominately *via* recoverable decorated surface complexation rather than irreversible elimination of functional groups which is consistent with previous results reported in amine functionalized mineral and silica sorbents.

Further confirmation of the integrity of operational NN@Slag is observed with top-view SEM micrographs (Fig. S2, SI). The as-prepared adsorbent shows rough, irregular granular morphology with abundant meso/macropores, which provides available sites for the stable uptake of Pb(II) ions, while the regenerated adsorbent retains its overall texture and particle size distribution without any severe agglomeration or cracking/collapse. Due to the observation that NN@Slag retains ~88% of its original Pb(II) removal efficiency after 5 consecutive adsorption–desorption cycles, these structural and spectroscopic results cumulatively reflect excellent stability of both the inorganic slag supporting backbone and definitely bound organosilane amine monolayer when subjected to used conditions. This durability complemented by high Langmuir capacity and favorable kinetics render NN@Slag a practically reusable waste derived adsorbent, even under regeneration protocols typical of Pb(II) remediation process in the real world.

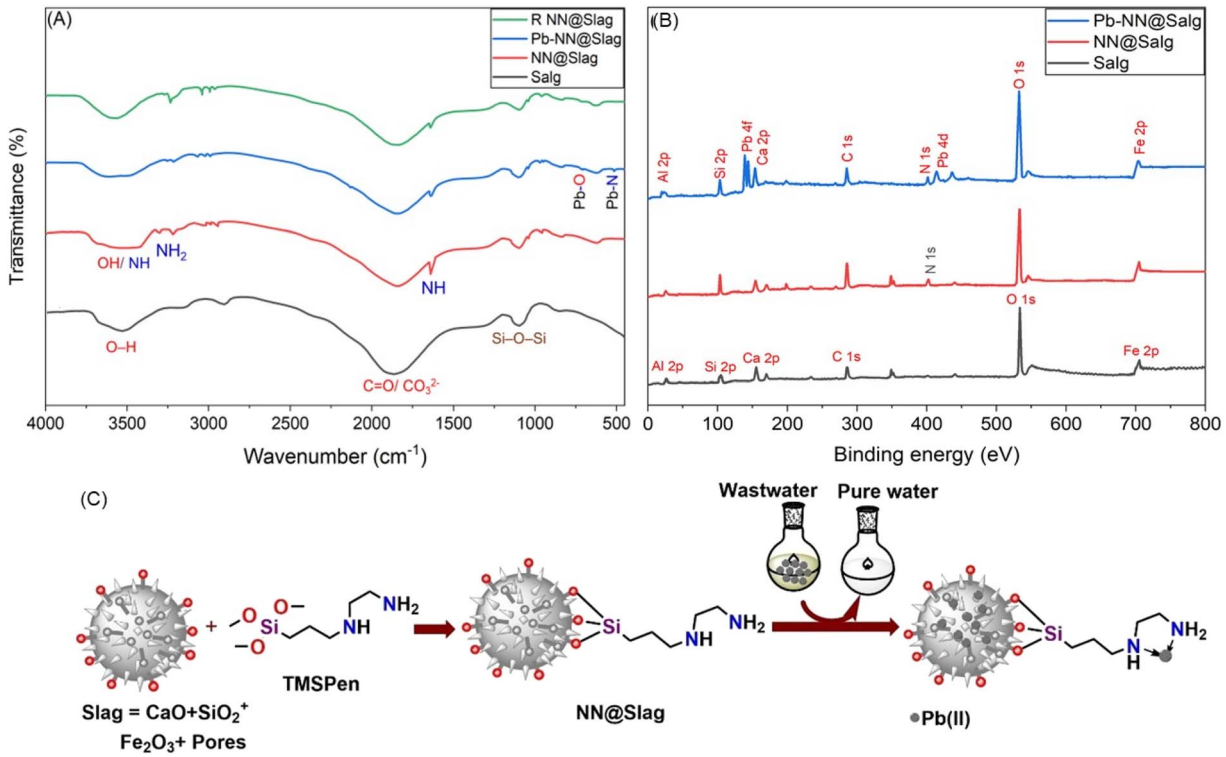

Fig. 9 (A) FTIR spectra of the pristine steel slag (slag), ethylenediamine-functionalized slag (NN@Salg) adsorbent, adsorbent after Pb(II) uptake (Pb-NN@Salg), and recovered adsorbent (R NN@Salg) after Pb(II) desorption. (B) XPS curves of slag, NN@Salg, and Pb-NN@Salg. (C) Schematic representation for the fabrication of the new adsorbent (NN@Slag) and the possible mechanism responsible for its performance in Cu(II) scavenging.

3.9. Adsorption mechanism

The FTIR spectra of the nascent adsorbent (NN@Slag) and Pb-loaded adsorbent (Pb-NN@Slag) (Fig. 9A), directly support the success of adsorption process as well as provide an insight into the mechanism of this process. Upon Pb(II) uptake (Pb-NN@Slag), the intensity of N–H/C–N band decreases and shifts as higher energy bands appear at low wavenumber in 500 to 700 cm^{-1} attributable to Pb–O/Pb–N coordination,[53] confirming amine and oxygen donor groups strongly coordinating with Pb(II) through inner sphere complexation instead of merely electrostatically interacting. Importantly, the FTIR spectrum of the regenerated adsorbent (R NN@Slag) closely mirrors that of the fresh NN@Slag: re-appearance of N–H/O–H and N–H/C–N bands re-intensifies while Pb–O/Pb–N features largely vanish, confirming that covalently bonded ethylenediamine still adheres to slag and also that Pb(II) is desorbed but without chemical degradation to its functional groups. Combined with the retained slag lattice bands, these IR signatures point to a strong reversible mechanism of chemisorption wherein Pb(II) is captured by amine and oxygen-bearing sites followed by desorption upon acid treatment further establishing NN@Slag as structurally stable and regenerable adsorbent for remediation of Pb(II).

Further, a direct, surface-sensitive evidence of successful grafting of ethylenediamine to slag and subsequent Pb(II) capture by the functionalized material were obtained from X ray photoelectron spectroscopy (XPS). As shown in Fig. 9B, pristine slag shows weak signals characteristic of its typical lattices (Ca 2p; Si 2p; Al 2p; Fe 2p; C 1s(adventitious carbon); O 1s) without any contribution detectable from nitrogen.[53] In contrast, the NN@Slag presents a distinct N 1s peak and increased Si 2p intensity is evident which is expected due to the formation of siloxane-anchored organic layer based on *N*(3 (trimethoxysilyl) propyl)ethylenediamine and terminal $–NH_2$/–NH groups are left exposed at surface. The transition from a purely inorganic (Si–O) to one containing N is quite consistent with earlier XPS studies on aminosilane-functionalized oxides and slags, in which the emergence of the N 1s alongside enhanced Si 2p features have been considered as unambiguous indicators for covalent grafting.

After Pb(II) adsorption, the spectrum of Pb-NN@Slag is characterized by the appearance of intense Pb 4f and Pb 4d doublets superimposed on existing Ca, Si, Al, Fe, C, N and O signals post adsorption confirming successful retention of Pb at adsorbent surface. Simultaneously, slight shifts and broadening of the N 1s and O 1s envelopes suggest that nitrogen and oxygen donors in the grafted layer engage in coordination to Pb(II), compatible with a chemisorption mechanism where complexation through Pb–N/O inner sphere is dominant over simple electrostatics. This XPS based evidence of metal–ligand bonding is also consistent with previously reported amine functionalized silica, carbon and slag systems and strengthens the basis for monolayer chemisorption established from the

Table 5 Comparison of adsorption performances of different reported adsorbents and that obtained in this study[a]

	Optimum adsorption conditions							
	pH	Time (h)	Dose (g L^{-1})	Temp. (K)	q_{max} (mg g^{-1})	Recyclability (cycle (n))	RE after n cycles (%)	Ref.
BFS	5.4	0.5	10.0	293	34.26	NA	NA	66
ASAC	4	48	20.0	298	22.8	NA	NA	67
SS	5	0.5	12.0	298	24.36	NA	NA	68
Kaolin	6	3.0	20.0	298	4.50	NA	NA	69
Bentonite	6	3.0	20.0	298	7.56	NA	NA	69
BFS	6	3.0	20.0	298	5.52	NA	NA	69
Fly ash	6	3.0	20.0	298	4.98	NA	NA	69
FGD ash	6	1.5	40.0	296	130.2	NA	NA	70
T-AC	5	4.0	0.5	298	268.61	NA	NA	71
MWCNTs/iron oxides/CD	5.5	24	0.4	293	12.3	5	95.44%	72
Oxidized MWCNTs	6.5	36	1.0	293	4.1	NA	NA	73
CGFS-PS-NH_2	5	3.0	1.0	298	113.90	5	87.62	74
CGFS-PS-SH	5	3.0	1.0	298	76.81	5	85.33	74
NN@Slag	6	1.5	0.8	298	108.04	5	87.79	TW

[a] RE: removal efficiency; ASAC: activated carbon prepared from apricot stone; SS: steel slag; FGD ash; dry desulfurization slag; T-AC: amino functionalized activated carbon derived from coal gasification fine slag; MWCNTs: multiwalled carbon nanotubes; CGFS-PS: coal gasification fine slag-functionalized porous silica; TW: this work.

Langmuir/PSO fitting. Collectively, the N 1s feature observed upon NN@Slag modification and the Pb 4f/4d signatures recorded postexposure to Pb(II) present a consistent picture whereby NN@Slag functions as a stable, covalently modified chelating surface with high-affinity binding to Pb(II), where the slag matrix remains intact.

Consequently, the possible mechanism for Pb(II) removal by TMSPen-modified slag (NN@Slag) involves multiple key steps. The grafting of slag by TMSPen results in the formation of NN@Slag through the introduction of ethylenediamine moieties, which are rich in amine ($-NH_2$) groups, onto the slag surface (refer to Fig. 9B). These functional groups provide active chelation sites capable of selectively binding Pb(II) ions from aqueous solutions. The complexation and immobilization of Pb(II) ions on the modified slag surface are facilitated by the strong coordination between the ions and the lone pairs of electrons on the nitrogen atoms within the ethylenediamine groups during adsorption. Additionally, the porous slag matrix enhances this chelation mechanism by offering a large surface area and accessibility for metal ions.

3.10. Rank of the new adsorbent compared reported ones

As shown in Table 5, NN@Slag exhibit a competitive performance with respect to Pb(II) removal and its Langmuir maximum capacity (108.04 mg g^{-1}) is obtained under mild conditions (pH 6; 1.5 h; 0.8 g L^{-1}; 298 K). This is more than threefold higher than that of common unmodified slag (5.52–34.26 mg g^{-1}) and greatly exceeds those of low-cost sorbents such as kaolin and fly ash (4.5–22.8 mg g^{-1}) used under high dosages (10–20 g L^{-1}). Although designed systems such as amino-functionalized activated carbon (T-AC, 268.61 mg g^{-1}) exhibit superior capacities, the needs of complex precursors, higher doses or more intense methods usually obscure their scalability and cost-effectiveness compared to NN@Slag.

Furthermore, NN@Slag is a good performer compared to other amorphous, amine-functionalized, slag-related materials. It indicates comparable capacity to CGFS-PS-NH_2 derived from coal gasification slag (113.90 mg g^{-1}) but lower solid loading (0.8 *vs.* 1.0 g L^{-1}) and shorter contact time (1.5 *vs.* 3 h), while similar recyclability in five cycles (87.79% *vs.* 87.62% removal efficiency). NN@Slag shows drastically better capacity (108.04 *vs.* 4.1–12.3 mg g^{-1}) than carbon-nanotube composites & oxidized MWCNTs, in addition to easier synthesis, shorter equilibration times and similar or even improved performance across cycles. This highlights its practical benefit over expensive nanoscale powders. In summary, NN@Slag typically outperformed low-cost adsorbents with established behavior in terms of capacity, dosage, contact time and reusability but deriving from a limitless steelmaking by-product and a commercially available silane. The multi-parameter performance and scalability of NN@Slag render it one of the most versatile adsorbents available for Pb(II) remediation and valuing-converter slag as a highly effective material in the state-of-the-art environmental applications.

4 Conclusion

This study utilized an innovative and economical method to create a highly efficient adsorbent for Pb(II) removal from wastewater. Blast furnace slag, a byproduct of the iron industry, served as a scaffold template for creating this adsorbent (NN@Slag) by grafting it with *N*-(3-(trimethoxysilyl)propyl)-ethylenediamine (TMSPen). The successful formation of NN@Slag as well its structural and morphological characteristics were elucidated based on the findings of spectroscopic and microscopic measurements. These analyses reveled the porous network of NN@Slag and scattering of the amine groups on the NN@Slag surface. The new adsorbent shows a promising

capability in scavenging of Pb(II) ions from aqueous effluents with maximum adsorption capacity of 108.04 mg g^{-1} under optimum conditions: pH 6, 90 min contact time, 0.04 g NN@Slag dosage, and Pb(II) initial concentration of 100 mg L^{-1}. In addition, the fitting of adsorption data exhibited a strong alignment with the Langmuir model ($R^2 = 0.98998$) and the pseudo-second-order kinetic model ($R^2 = 0.98544$), indicating a homogeneous adsorption process governed by chemisorption mechanisms, which underscores the adsorbent's efficacy and suggests its suitability for practical applications in mitigating Pb(II) pollution in aqueous environments.

While NN@Slag possesses a high Pb(II) removal efficiency and favorable regenerability, the environmental safety of NN@Slag needs to be assessed for potential leaching from intrinsic slag components as well as the stability of grafted amine layer under realistic operating conditions before large-scale utilization. This said, future efforts will be directed towards standardized leaching and ecotoxicity (*e.g.*, bioassays) tests to ensure that the technical use-mined NN@Slag and their disposal do not pose secondary contamination hazards in treated waters or in receiving environmental compartments.

Another limitation of this study is that the leaching of intrinsic slag metals (including thus far unknown values for Fe, Mn and Cr) during adsorption–desorption ciclo-destructive cycles was not quantified since our investigation and available resources were focused on Pb(II) removal performance (full characterization of the leachate fell out of the scope). Future studies will include systematic analyses of treated solutions and eluates, using standardized leaching and ecotoxicity tests to elucidate the release of these elements from NN@Slag under realistic operational conditions as well to evaluate whether its application entails secondary contamination risks.

Conflicts of interest

The authors declare no competing interests.

Data availability

The datasets generated and/or analyzed during the current study are available from the corresponding author on reasonable request.

Supplementary information (SI) is available. See DOI: https://doi.org/10.1039/d6ra00707d.

Acknowledgements

This work was supported and funded by the Deanship of Scientific Research at Imam Mohammad Ibn Saud Islamic University (IMSIU) (grant number IMSIU-DDRSP2602).

References

1 A. Kumar, V. Kumar, M. Thakur, K. Singh, R. Jasrotia, R. Kumar and M. Radziemska, *Land Degrad. Dev.*, 2025, **36**, 2159–2169.
2 R. Yahya and R. F. M. Elshaarawy, *Int. J. Biol. Macromol.*, 2024, **277**, 134350.
3 O. World Health, *Exposure to Lead: a Major Public Health Concern. Preventing Disease through Healthy Environments*, World Health Organization, 2025.
4 Y. Han, S. Zhang, D. Kang, N. Hao, J. Peng, Y. Zhou, K. Liu and Y. Chen, *Water, Air, Soil Pollut.*, 2025, **236**, 144.
5 B. Kamal and A. Rafey, *Int. J. Environ. Anal. Chem.*, 2023, **103**, 5126–5141.
6 A. M. Taha, F. H. A. Mustafa, H. E. Ibrahim, L. I. Mohamadein, Z. M. Anwar and R. F. M. Elsharaawy, *Int. J. Biol. Macromol.*, 2025, 143846.
7 N. Abdus-Salam and F. A. Adekola, *Afr. J. Sci. Technol.*, 2005, **6**, 55–66.
8 M. Ahrouch, J. M. Gatica, K. Draoui, D. Bellido and H. Vidal, *J. Hazard. Mater.*, 2019, **365**, 519–530.
9 J. A. Alexander, M. A. Ahmad Zaini, A. Surajudeen, E.-N. U. Aliyu and A. U. Omeiza, *Part. Sci. Technol.*, 2018, **36**, 569–577.
10 L. Khalfa, A. Sdiri, M. Bagane and M. L. Cervera, *J. Cleaner Prod.*, 2021, **278**, 123935.
11 Z. Esvandi, R. Foroutan, M. Mirjalili, G. A. Sorial and B. Ramavandi, *J. Polym. Environ.*, 2019, **27**, 263–274.
12 S.-H. Kim, H. Song, G. M. Nisola, J. Ahn, M. M. Galera, C. hee Lee and W.-J. Chung, *Adsorption*, 2006, **4**, 6.
13 N. S. Ahmedzeki, *Desalin. Water Treat.*, 2013, **51**, 5559–5565.
14 H. Namkoong, E. Biehler, G. Namkoong and T. M. Abdel-Fattah, *ACS Omega*, 2022, **7**, 39931–39937.
15 A. Mlayah, S. Jellali, A. A. Azzaz, M. Jeguirim, H. Sellalmi and N. Hamdi, *C. R. Chim.*, 2021, **24**, 7–22.
16 P. K. Pandey, S. K. Sharma and S. S. Sambi, *J. Environ. Chem. Eng.*, 2015, **3**, 2604–2610.
17 R. Senthilkumar, K. Vijayaraghavan, M. Thilakavathi, P. V. R. Iyer and M. Velan, *Biochem. Eng. J.*, 2007, **33**, 211–216.
18 B. Yu, Y. Zhang, A. Shukla, S. S. Shukla and K. L. Dorris, *J. Hazard. Mater.*, 2001, **84**, 83–94.
19 A. Awad, *Results Eng.*, 2024, **22**, 102311.
20 W. Astuti, A. Chafidz, A. S. Al-Fatesh and A. H. Fakeeha, *Chin. J. Chem. Eng.*, 2021, **34**, 289–298.
21 Z. B. Bouabidi, M. H. El-Naas, D. Cortes and G. McKay, *Chem. Eng. J.*, 2018, **334**, 837–844.
22 V. K. Gupta and I. Ali, *J. Colloid Interface Sci.*, 2004, **271**, 321–328.
23 V. K. Gupta, M. Gupta and S. Sharma, *Water Res.*, 2001, **35**, 1125–1134.
24 S. V. Dimitrova and D. R. Mehandgiev, *Water Res.*, 1998, **32**, 3289–3292.
25 B. Tijjani, A. L. Yaumi, H. D. Mohammed, H. Umar, E. Yakubu and B. K. Highina, *Int. J. Environ.*, 2024, **13**, 21–47.
26 P. C. Mishra, M. Islam and R. K. Patel, *Sep. Sci. Technol.*, 2013, **48**, 1234–1242.
27 I. R. Chowdhury, S. Chowdhury, M. A. J. Mazumder and A. Al-Ahmed, *Appl. Water Sci.*, 2022, **12**, 185.
28 A. Ehrenberg, *ce/papers*, 2023, vol. 6, pp. 241–256.
29 D. M. Proctor, K. A. Fehling, E. C. Shay, J. L. Wittenborn, J. J. Green, C. Avent, R. D. Bigham, M. Connolly, B. Lee

and T. O. Shepker, *Environ. Sci. Technol.*, 2000, **34**, 1576–1582.
30 A. Heidari, H. Younesi and Z. Mehraban, *Chem. Eng. J.*, 2009, **153**, 70–79.
31 R. Fu, Y. Liu, Z. Lou, Z. Wang, S. A. Baig and X. Xu, *J. Taiwan Inst. Chem. Eng.*, 2016, **62**, 247–258.
32 K. Yang, Z. Lou, R. Fu, J. Zhou, J. Xu, S. A. Baig and X. Xu, *J. Mol. Liq.*, 2018, **260**, 149–158.
33 L. Qin, L. Yan, J. Chen, T. Liu, H. Yu and B. Du, *Ind. Eng. Chem. Res.*, 2016, **55**, 7344–7354.
34 G. Li, B. Wang, Q. Sun, W. Q. Xu and Y. Han, *Microporous Mesoporous Mater.*, 2017, **252**, 105–115.
35 Y. Liu, J. Xu, Z. Cao, R. Fu, C. Zhou, Z. Wang and X. Xu, *J. Colloid Interface Sci.*, 2020, **559**, 215–225.
36 Y. Tan, K. Wang, Q. Yan, S. Zhang, J. Li and Y. Ji, *ACS Omega*, 2019, **4**, 10475–10484.
37 S. Vallinayagam, K. Rajendran, S. K. Lakkaboyana, K. Soontarapa, R. R. R, V. K. Sharma, V. Kumar, K. Venkateswarlu and J. R. Koduru, *J. Environ. Chem. Eng.*, 2021, **9**, 106553.
38 W. Abd El-Fattah, A. Guesmi, N. B. Hamadi, R. Yahya, T. S. Alraddadi, A. Shahat and R. F. M. Elshaarawy, *RSC Adv.*, 2025, **15**, 33695–33707.
39 N. Y. Elamin, M. R. Elamin, L. S. Alqarni, R. O. Yahya, A. Shahat and R. F. M. Elshaarawy, *React. Funct. Polym.*, 2025, 106423.
40 M. A. Rizk, R. A. Alsaiari, A. Shahat, M. A. Alsaiari, R. F. M. Elshaarawy and A. S. Taha, *J. Mol. Liq.*, 2023, 123086.
41 D. Mombelli, A. Gruttadauria, S. Barella and C. Mapelli, *Minerals*, 2019, **9**, 706.
42 M. R. Nilforoushan, *Asian J. Water, Environ. Pollut.*, 2009, **6**, 31–36.
43 L. Plaza, M. Castellote, R. Nevshupa and E. Jimenez-Relinque, *Environ. Sci. Pollut. Res.*, 2021, **28**, 23896–23910.
44 B. Han, S. Ding, J. Wang and J. Ou, in *Nano-Engineered Cementitious Composites: Principles and Practices*, Springer, 2019, pp. 1–96.
45 C. Ma, S. Zhang, K. Li, T. Zhao, Q. Meng, D. Guan and A. Zhang, *Metals*, 2025, **15**, 537.
46 H. Bahramnia, H. Mohammadian Semnani, A. Habibolahzadeh, H. Abdoos and F. Rezaei, *Fullerenes, Nanotubes Carbon Nanostruct.*, 2021, **29**, 74–82.
47 M. S. Hameed, S. D. P. Antony, R. Shanmugam and S. Raghu, *J. Int. Oral Health*, 2024, **16**, 386–393.
48 Y. Tan, M. Chen and Y. Hao, *Chem. Eng. J.*, 2012, **191**, 104–111.
49 Y. Zhang, L. Magagnin, K. Yuan, Z. Wei, X. Wu, Z. Jiang and W. Wang, *Microporous Mesoporous Mater.*, 2022, **345**, 112280.
50 M. D. Donohue and G. L. Aranovich, *Adv. Colloid Interface Sci.*, 1998, **76**, 137–152.
51 K. S. W. Sing, *Pure Appl. Chem.*, 1985, **57**, 603–619.
52 Y. Wang, H. Li, S. Cui and Q. Wei, *Water*, 2021, **13**, 2735.
53 L. Ren, Y. Gong, R. Wu, Q. Guo, G. Yu and F. Wang, *Sep. Purif. Technol.*, 2025, **369**, 133162.
54 Y. Zhou, S. Xia, J. Zhang, B. T. Nguyen and Z. Zhang, *Chem. Eng. J.*, 2017, **308**, 1098–1104.
55 K. Manzoor, M. Ahmad, S. Ahmad and S. Ikram, *RSC Adv.*, 2019, **9**, 7890–7902.
56 C. Toufik, K. Ouahida, C. Sana and B. Aatmane, *Anal. Bioanal. Chem. Res.*, 2023, **10**, 251–268.
57 S. M. Abdelbasir and M. A. A. Khalek, *Environ. Sci. Pollut. Res.*, 2022, **29**, 57964–57979.
58 B. Li, J.-L. Liu and H. Xu, *Environ. Sci. Pollut. Res.*, 2022, **29**, 49808–49815.
59 P. Kumkum and S. Kumar, *Biomass*, 2024, **4**, 243–272.
60 N. K. Asmel, A. R. M. Yusoff, L. Sivarama Krishna, Z. A. Majid and S. Salmiati, *Chem. Eng. J.*, 2017, **317**, 343–355.
61 S. Azizian, S. Eris and L. D. Wilson, *Chem. Phys.*, 2018, **513**, 99–104.
62 K. Y. Foo and B. H. Hameed, *Chem. Eng. J.*, 2010, **156**, 2–10.
63 K. H. Chu, *Ind. Eng. Chem. Res.*, 2021, **60**, 13140–13147.
64 S. K. Lakkaboyana, S. Khantong, N. K. Asmel, S. Obaidullah, V. Kumar, K. Kannan, K. Venkateswarlu, A. Yuzir and W. Z. Wan Yaacob, *J. Environ. Chem. Eng.*, 2021, **9**, 106483.
65 J. Madejová, *Vib. Spectrosc.*, 2003, **31**, 1–10.
66 T. Chouchane, S. Chibani, O. Khiriddine and A. Boukari, *Iran. J. Mater. Sci. Eng.*, 2023, **20**, 1.
67 M. Kobya, E. Demirbas, E. Senturk and M. Ince, *Bioresour. Technol.*, 2005, **96**, 1518–1521.
68 L. Wang, P. Fu, Y. Ma, X. Zhang, Y. Zhang and X. Yang, *Miner. Eng.*, 2022, **183**, 107593.
69 P. C. Mishra and R. K. Patel, *J. Hazard. Mater.*, 2009, **168**, 319–325.
70 Q. Wu, R. You, M. Clark and Y. Yu, *Appl. Surf. Sci.*, 2014, **314**, 129–137.
71 B. Liu, P. Lv, Q. Wang, Y. Bai, J. Wang, W. Su, X. Song and G. Yu, *J. Environ. Chem. Eng.*, 2024, **12**, 112635.
72 J. Hu, D. Shao, C. Chen, G. Sheng, J. Li, X. Wang and M. Nagatsu, *J. Phys. Chem. B*, 2010, **114**, 6779–6785.
73 D. Xu, X. Tan, C. Chen and X. Wang, *J. Hazard. Mater.*, 2008, **154**, 407–416.
74 L. Ren, Y. Gong, R. Wu, Q. Guo, G. Yu and F. Wang, *Sep. Purif. Technol.*, 2025, **369**, 133162.